Cimifugin Suppresses NF-κB Signaling to Prevent Osteoclastogenesis and Periprosthetic Osteolysis

Juan Duan
Second Xiangya Hospital
Xuantao Hu
Second Xiangya Hospital Department of Orthopedics
Tao Li
Second Xiangya Hospital Department of Orthopedics
Pengcheng Dou (doupengcheng@csu.edu.cn)
Second Xiangya Hospital Department of Orthopedics https://orcid.org/0000-0003-3719-4040

Research article

Keywords: CIM, osteoclast, NF-κB, p38, MAPK, aseptic prosthetic loosening, periprosthetic osteolysis

Posted Date: May 11th, 2021

DOI: https://doi.org/10.21203/rs.3.rs-495643/v1

Abstract

Background: Aseptic loosening of prosthesis (ALP) is one of the most common long-term complication of knee and hip arthroplasty. Wear paticle-induced osteoclastogenesis and subsequent periprosthetic osteolysis accounts for the morbidity of ALP. Here, we investigate cimifugin (CIM), a natural extract from *Cimicifuga Racemosa* and *Saposhnikovia Divaricata*, as a bone protective drug in treatment of ALP.

Method: First, we deployed cell viability and osteoclast formation assays to detect the effect of noncytotoxic CIM on osteoclast differentiation *in vitro*. Bone slice resorption evaluation and F-actin ring immunofluorescence assays were adopted to measure bone-resorbing function affected by CIM. Then, we introduce quantitative real-time polymerase chain reaction (qRT-PCR) analysis to further identify the repressed osteoclastogenesis by CIM in gene expression level. To reveal underlying mechanism of findings above, we used Western blotting and luciferase reporter gene assay to determine the regulation manner of CIM in NF-κB and MAPKs signaling pathways. Moreover, Ti particle-induced murine calvarial osteolysis model and following histomorphometric analysis via micro-CT and immunohistochemical staining were used to demonstrate the effect of CIM on periprosthetic osteolysis *in vivo*.

Result: CIM administration dose-dependently inhibited both bone marrow-derived macrophages (BMMs) and RAW264.7 cells derived osteoclastogenesis and bone resorption pit formation *in vitro*, which further supported by reduced expression of F-actin and osteoclast specific genes. According to the Western blotting analysis, inhibition of IkBa phosphorylation in NF-κB signaling pathway, not the phosphorylation of MAPKs, was detected as the suppressive effect of CIM on osteoclastogenesis. In vivo animal experiment demonstrated that CIM alleviated Ti particle-induced bone erosion and osteoclast accumulation in murine calvaria.

Conclusion: The current study for the first time proved that CIM could dose-dependently inhibit RANKL-induced osetoclastogenesis via suppressing NF-κB signaling pathway *in vitro* and prevent periprosthetic osteolysis *in vivo*. These findings suggest the potential therapeutic use of CIM in ALP.

1 Introduction

With the development of prosthesis design and minimally invasive procedure, arthroplasty has become one of the most reliable surgery to treat diseases of most intractability, such as severe osteoarthritis, developmental dysplasia of the hip, old femoral neck fracture and arthropathy of rheumatoid or ankylosing spondylitis. In recent decades, people received arthroplasty surgery in worldwide has been growing with hundreds of thousands per year. Research suggests that, about 5% patients develop aseptic loosening of prosthesis (ALP) after receiving arthroplasty and require complicated revision surgery [1]. To avoid this, great efforts have been made to find the therapies for ALP.

The pathophysiology of ALP has been mainly attributed to the following two aspects: the “stress shielding” caused by prosthesis of high rigidity, and the wear particles produced by the friction between implants and host bone especially [2; 3]. Generally, nanoparticles shed from Ti, Co and Cr based metal,

polyethylene, bone cement and ceramic implants trigger inflammatory response in periprosthetic tissue [4; 5]. Cell lineages including macrophages, osteoblasts, osteoclasts, mesenchymal stem cells participate in the mechanism network and raise a surge of pro-inflammatory factors, which contains reactive oxygen species, chemokines, TNF-α, IL-1β and IL-6 [6]. Notably, the disrupted osteoblast metabolism causes the imbalance of receptor activator of nuclear factor κ B ligand (RANKL)- osteoprotegerin (OPG) [7]. The excessive RANKL triggers the formation of osteoclasts via binding to the receptor activator of nuclear factor κ B (RANK) located on the surface of cell membrane and consequently produce an initial signal to recruit TNF receptor-associated factor 6 (TRAF6) [8]. Activated TRAF6 promotes nuclear factor-κB (NF-κB) and mitogen-activated protein kinases (MAPKs) signaling cascades, which lead to the upregulation of osteoclast marker genes including Nfatc1, Calcr, Cathepsin K, etc. As the result, bone-resorbing effect mediated osteoclast was enhanced and periprosthetic osteolysis occurs [8]. Therefore, wear-debris-induced inflammatory response and pathological formation of osteoclast in periprosthetic tissue play pivotal roles in the occurrence of ALP.

To prevent ALP, the design prosthesis for total hip arthroplasty has been improved over several generations to guarantee the proper stress distribution and less abrasion between interfaces by adopting biochemical-conforming shape and materials of higher biocompatibility. However, for patients with risk factors or those who have already developed early stage ALP, the effects of existing treatments are less than satisfactory [9]. Given this, we investigated a natural compound called Cimifugin (CIM) as one of main components of *Saposhnikovia Divaricata* or *Cimicifuga Racemosa* extract [10; 11]. CIM is commonly reported as a bioactive chromone independently or in multiple Chinese medicine formulae with reported properties of antinociception, antiinflammation and lipid metabolism regulation in a spectrum of diseases, including allergy in skin and respiratory system, inflammatory arthropathies, and cerebral ischemia by inhibiting the production of inflammatory factors and NF-kb/MAPK signaling [11–16]. However, in term of the treatment for ALP, the bioactivity of CIM has not been investigated in osteoclastogenesis and subsequent periprosthetic osteolysis. Also, the involved molecular mechanism in osteoclast and its precursors remains elusive.

To this end, we deployed a range of experiment in the current study and attempted to 1) investigate the effect of CIM on osteoclast differentiation, 2) detect the therapeutic activity for Ti particle-induced periprosthetic osteolysis by CIM and 3) elucidate to underlying molecular mechanism. The current findings suggest an extension of natural compound spectrum for ALP prevention or conservative treatment.

2 Materials And Methods

2.1 Cell Culture and Main Reagents

Cell lineages used in the present study include osteoclast precursor RAW 264.7 and primary bone marrow monocytes (BMMs) of murine. RAW264.7 cells were obtained from the inventory of the Orthopedic

Laboratory of the Second Xiangya Hospital. RAW264.7 cells was cultured in standard Alpha-modified minimal essential medium (α-MEM) (Gibco-BRL; Beijing, China) supplemented with 10% fetal bovine serum (FBS) (Gibco-BRL; Scotland, UK) and 1% penicillin/streptomycin, namely complete α-MEM (c-α-MEM). The standard cell culture conditions were constant 37 ℃, 5% CO_2 humid atmosphere in incubator [17]. The isolation procedure of BMMs was described in previous study [18]. In brief, bone marrow was harvested from the bone shafts of male, four- to six-week-old C57BL/6 mice and cultured in c-α-MEM with an addition of 10 ng/mL macrophage colony-stimulating (M-CSF) (R&D Systems; Minneapolis, MN, USA) for 24 h. Then, non-adherent cells were removed and the adherent cells (primary BMMs) were continuously incubated in fresh c-α-MEM with M-CSF for 72–96 h until the confluence of cells was observed. The medium and incubation conditions used in the present study remained unchanged unless stated otherwise.

CIM ($C_{16}H_{18}O_6$, 306.310, purity ≥ 99%) were purchased from Yuanye Biology Ltd. (Shanghai, China) and dissolved in α-MEM at 80 mM as storage solution saved at 4 ℃ away from light. RANKL was acquired from R&D Systems (Minneapolis, MN, USA). The cell counting kit (CCK-8) was supplied by Dojindo Molecular Technology (Shanghai; China). The tartrate-resistant acid phosphatase (TRAP) staining kit were purchased from Sigma Aldrich (St Louis, MO, USA). Primary and secondary antibodies for western blotting and immunohistochemistry were purchased from Cell Signaling Technology (Cambridge, MA, USA). Qiagen RNeasy Mini kit (Qiagen, Valencia, CA, USA), reverse transcriptase (TaKaRa Biotechnology, Otsu, Japan) SYBR Premix Ex Tag kit (TaKaRa, Biotechnology, Otsu, Japan) was used in quantitative PCR.

2.2 Cell Viability

To determine the cytotoxicity of CIM, RAW264.7 or BMMs cells were seeded at 3 ×10^3/well in triplicates in 96-well plates and incubate overnight for adhesion. Then, cells were treated with CIM of gradient concentrations (0, 10, 20, 40, 80, 160, 320, 640, 1280, 2560 mM) in the medium for 48 or 96 h respectively. The medium was replaced every 48 h. Then, the medium in each well was replaced with 100 ul fresh medium containing 10% CCK-8 buffer solution, and the 96-well plates were incubated in the same conditions for 1 h. The absorbance was measured at a wavelength of 450 nm with phosphate buffer saline (PBS) well as reference using ELX800 absorbance microplate reader (Bio-Tek, USA) [19]. Cell viability was calculated relative to the vehicle-treated control group in percentage.

2.3 Osteoclast Formation Assay

For osteoclast differentiation assessment *in vitro*, we seeded RAW264.7 or BMMs cells at a density of 2.0×10^3 cells/well in triplicates and treated with medium containing CIM of varying concentrations (0, 80, 160, 320 mM) and 50 ng/ml RANKL. The medium was replaced every 24 h for 5–7 days until multi-nuclear giant cells were clearly observed. Cells were then rinsed twice with PBS and fixed with 4% paraformaldehyde for 20 min. After removing the paraformaldehyde solution, the TRAP staining procedure was conducted according to the instruction book. TRAP-positive cells with more than three

nuclei were counted under a microscope, and the images were captured for measurements using Image J software (NIH, Bethesda, MD, USA).

2.4 Resorption Pit Formation Assay

Bovine bone slices placed in wells of 96-well plates after being sterilized and dried. RAW264.7 cells (2.0×10^3 cells/well) were seeded at 2.5×10^3 cells/well onto bone slices in triplicates and treated with 50 ng/ml RANKL and CIM (0, 80, 160, 320 mM) for 7 days until mature osteoclasts formed. Then, cells on the bone slices were removed with brushing and sonication. The osteolytic surfaces of bone slices were visualized under the scanning and imaging of a scanning electron microscope (SEM; FEI Quanta 250). The captured images were analyzed using Image J software for bone resorption evaluation.

2.5 F-actin Ring Immunofluorescence Assay

To further quantify the effect of CIM on osteoclasts activity, BMMs were treated with 50 ng/mL of RANKL and different concentrations of CIM (0, 80, 320 mM), which is identical to the cell preparation before TRAP staining in the osteoclast formation assay as previously described. Cell samples were permeabilized with PBS containing 0.1% Triton X (Sigma Aldrich, St Louis, MO, USA) for 5 min. Then, cells were incubated with Alexa-Fluor 647 phalloidin (Invitrogen, San Diego, CA, USA) diluted in 0.2% (w/v) BSA-PBS (Invitrogen, San Diego, CA, USA) for 1 h in darkness. After extensively rinsing with PBS, cells were mounted with ProLong Gold anti-fade mounting medium (Invitrogen, San Diego, CA, USA) to visualize cell nuclei [20]. We used a NIKON A1Si spectral detector confocal system (Nikion, Tokyo, Japan) with the systems NISC Elements software to acquire fluorescence images, and the numbers of F-actin were quantified using Image J software.

2.6 RNA Isolation and Quantitative Real-Time Polymerase Chain Reaction (qRT-PCR) Analysis

We deployed qRT-PCR analysis to determine the osteoclast differentiation on transcriptional level. BMMs (1.0×10^5 cells/well) were seeded in 24-well plates in triplicates and administered with c-α-MEM containing 30 ng/ml M-CSF, 50 ng/ml RANKL and different doses of CIM (0, 80, 160, 320 mM) for 5 days. Total RNA of different groups was extracted respectively with the Qiagen RNeasy Mini kit (Qiagen; Valencia, CA, USA) by following the operating instructions. Then, 1 mg of total RNA was reverse-transcripted using a reverse transcriptase kit (TaKaRa Biotechnology; Otsu, Japan) to produce cDNAs (complementary DNAs), which served as templates of for following qRT-PCR assay using an SYBR Premix Ex Tag kit (TaKaRa Biotechnology) and an ABI 7500 Sequencing Detection System (Applied Biosystems; Foster City, CA, USA). qRT-PCR was conducted for 40 cycles with denaturation at 95°C for 5 s and amplification at 60°C for 34 s, and the levels of osteoclast specific genes were normalized with Gapdh as internal reference. The murine primer sequences were listed in Table 1.

Table 1
Murine primer sequences for quantitative real-time PCR analysis

Gene	Forward primer (5'-3')	Reverse primer (3'-5')
c-Fos	CCAGTCAAGAGCATCAGCAA	AAGTAGTGCAGCCCGGAGTA
Trap6	AAACCACGAAGAGGTCATGG	GCGGGTAGAGACTTCACAGC
Acp5	TCCTGGCTCAAAAAGCAGTT	ACATAGCCCACACCGTTCTC
Calcr	CGGACTTTGACACAGCAGAA	AGCAGCAATCGACAAGGAGT
Cathepsin K	CTTCCAATACGTGCAGCAGA	TCTTCAGGGCTTTCTCGTTC
Nfatc1	CCGTTGCTTCCAGAAAATAACA	TGTGGGATGTGAACTCGGAA
Dc-stamp	AAAACCCTTGGGCTGTTCTT	AATCATGGACGACTCCTTGG
Gadph	ACCCAGAAGACTGTGGATGG	CACATTGGGGGTAGGAACAC

2.7 Western Blotting Analysis

To elucidate the effect of CIM on the RANKL-induced osteoclast signaling, we seeded RAW264.7 cells at 5.0×10^5 cells/well in 6-well plates. After being confluent, the cells were pretreated with α-MEM containing 320 mM CIM or not for 4 h followed by stimulation of a-MEM containing 50 ng/ml RANKL for 0, 5, 10, 20, 30, or 60 min. The total proteins were isolated from the cultured cells using the radioimmunoprecipitation assay (RIPA) lysis buffer (Beyotime, Shanghai, China) supplemented phenylmethysulfonyl fluoride (PMSF) followed by centrifugation at 12,000× g for 15 min. The supernatant enriched with protein products were collected quantified with a bicinchoninic acid assay kit (Biosharp Life Science, China) according to the instructions. Next, the protein products (30 mg) from each group were separated using sodium dodecyl sulfatepolyacrylamide gel electrophoresis (SDS-PAGE) on 10% gels and then transferred to PVDF membranes (Millipore, Bedford, MA, USA). After being blocked in 5% (w/v) skimmed milk powder in TBS-Tween (Tris-buffered saline-Tween: 0.1% Tween-20 in TBS) at room temperature for 1 h, the PVDF membranes were incubated for 12 h at 4°C with primary antibodies including Nuclear factor of kappa light polypeptide gene enhancer in B-cells inhibitor alpha (IkBa), p-IkBa, JNK, p-JNK, ERK, p-ERK, p38, p-p38 and b-actin (Cell Signaling Technology, Cambridge, MA, USA). Then, the membranes were rinsed and incubated with corresponding secondary antibodies at room temperature for 1 h. Antibody reactivity and protein bands were detected by exposure in an Odyssey V3.0 imaging system (LI-COR, Lincoln, NE, USA). Band intensity of the images were quantified using Image J software.

2.8 Luciferase Reporter Gene Assay

To further investigate the inhibition effect of CIM on RANKL-induced activation of NF-κB, the NF-κB luciferase reporter *3kB-Luc-SV40* was constructed and stably transfected into RAW264.7 cells as described before[21]. The cells were then seeded into 48-well plate and incubated for 24 h for adhesion and

subsequently treated with CIM at the concentration of 0, 80, 320 mM. Then, we administered 50 ng/mL RANKL to each well and incubated for another 8 h. Luciferase activity reflected by the fluorescence intensity detected with Promega Luciferase Assay System (Promega, Madison, WI, USA) and controlled by vehicle group [22].

2.9 Ti Particle-Induced Murine Calvarial Osteolysis Model

Commercial Ti particles with diameter at 4.5 mm in average were purchased from Johnson Matthey (Ward Hill, MA,USA). Particles were baked for 6 h at 180°C, then immersed with 75% ethanol and shook for 24 h for endotoxin removal. Ti particles were resuspended with sterile PBS at 0.3 g/ml and confirmed to be free of endotoxins via a Limulus amebocyte lysate assay before being storage at 4°C.

For animal experiment, the protocol was performed in accordance with the recommendations of guiding principles of Animal Care Committee of Central South University and approved by the Animal Care Committee of Central South University.

Eighteen 6-8-week-old C57BL/6 male mice (weight: 22.64 ± 1.54g) were acquired from Shanghai Slac Laboratory Animal Company and raised in 3 specific pathogen-free (SPF) cages with 6 mice in each group: mice recieved sham operation and PBS treatment (sham group), those received Ti particles implantation and PBS treatment (vehicle group), and those received Ti particles implantation and 50 mg/kg CIM (CIM group). Before surgical operation, the mice underwent anesthesia with intraperitoneal delivery of 4% chloral hydrate at 0.1ml/10g•bw. The cranial periosteum was cleaved with median incision and sutured with 30 mg Ti particles embedded between the periosteum and the calvarium [23].After first 2 days, mice in CIM group received 50 mg/kg intragastrical CIM every 2 days and in sham and vehicle group PBS for 8 weeks. Finally, the mice were euthanized 2 days after the last treatment for calvaria harvest. The calvaria samples were fixed with 4% paraformaldehyde followed by micro-computed tomography (micro-CT) analysis.

2.10 Micro-CT Scanning

A high-resolution micro-CT system (μCT50; Scanco; Zurich; Switzerland) was deployed to detected the morphology of calvarial osteolysis. The scanning was conducted under 10 μm isometric resolution, 300 ms exposure time, and 80 kV, 80 mA X-ray energy. The reconstructed images of calvarial surface around median incision as region-of-interest were obtained and analyzed for morphologogical parameters including bone mineral density (BMD), bone volume against tissue volume (BV/TV), the number of pores, and percentage of total porosity.

2.11 Immunohistochemical Staining and Histomorphometric Analysis

After being scanned with micro-CT, the fixed calvaria samples were decalcified using 10% EDTA for 3 weeks and embedded in paraffin. Then, the samples were sectioned serially and underwent TRAP and

H&E staining. The images were collected using high quality microscopy followed by the quantification of TRAP-positive multinucleated osteoclasts using Image J software.

2.12 Statistical Analysis

The data of each experiments were acquired from at least three replications and presented in the form of means ± SD (standard deviation). Data analyses were performed using the Student's t-test in the SPSS 20.0 software (SPSS Inc., USA). Significant difference between the results of different groups were marked as * for $P < 0.05$ and ** for $P < 0.01$.

3 Results

3.1 CIM of Noncytotoxic Dose Repressed Osteoclastogenesis *in Vitro*

The chemical structural formula of CIM was presented in Fig. 1A. To avoid repressed osteoclast formation caused by cytotoxicity of CIM, the noncytotoxic concentration of CIM in osteoclast precursors was identified. The result suggested that CIM over 640 mM significantly reduced the number osteoclast precursors, while CIM below 320 mM didn't, indicating a noncytotoxic threshold of 320 mM for following osteoclast assays (Fig. 1B).

Then, the inhibited RANKL-induced osteoclast formation by CIM was investigated *in vitro*. As is shown in Fig. 1C and E, excessive TRAP + mature multinucleated giant cells with distinct cytoplasm identified as osteoclasts were observed in both RAW264.7 and BMMs cell lineages. However, the number and area of osteoclasts in groups treated CIM of varying concentrations were dose-dependently decreased (Fig. 1C-E). It seems that 320 mM CIM exerted a significant inhibition on the osteoclastogenesis especially in RAW264.7 group.

3.2 CIM Attenuated Bone-Resorbing Function of Mature Osteoclasts *in Vitro*

Given the inhibited osteoclastogeneis by CIM, we assumed a paralleled decrease in bone-resorbing function of osteoclast induced by CIM. To approve this, bone slice resorption assay was established. As demonstrated in the Fig. 2A and B, RANKL-induced formation of resorption pits was clearly observed on the surface of interest in the control group, while CIM treatment led to a decrease of resorption pit area with the increasing concentration as expected. According to the quantification result, the resorption pit area decreased about 85% relative to the control after being treated with 320 mM CIM.

F-actin ring in cytoplasm is widely recognized as an indicator of functional osteoclasts in bone resorption [24]. Therefore, we quantified the F-actin in CIM treated osteoclasts using immunofluorescence assay. As shown in Fig. 2C and D, F-actin rings were well polarized along with RANKL-induced osteoclastogenesis,

while CIM treatment reduced the number and area of F-actin rings, which further proved the repressed function of osteoclast caused by CIM administration. In summary, these data suggested that noncytotoxic CIM is of inhibitory effect on osteoclast formation and bone-resorbing function.

3.3 CIM Inhibits Expression of Osteoclast Specific Genes *in Vitro*

Stimulation of RANKL always activated the excessive expression of specific genes and subsequent differentiation towards osteoclast in osteoclast precursors. Therefore, we performed qRT-PCR to detect transcriptional quantity of osteoclast-specific genes affected by CIM. As indicated in Fig. 3, the high transcription of specific genes encoding key factors and markers of osteoclastogenesis, including c-Fos, Nfatc1, Acp5, Calcr, Cathespin K, Dc-stamp and Traf6, were dose-dependently diminished by the treatment of CIM. These results further supported the repressive effect of CIM on osteoclastogenesis and bone-resorbing function.

3.4 CIM Alleviated RANKL-Induced NF-κB Signaling in Osteoclastogenesis *in Vitro*

To unveil the underlying molecular mechanism involved in the anti-osteoclastogenetic property, Western blotting was deployed to measure the time-dependent expression of key factors mediating NF-κB and MAPKs (JNK, ERK, and p38) signaling cascades in RANKL-induced osteoclastogenesis.

As reflected by the serial bands in Fig. 4A and B, the p-IkBa peaked within 5 min in control group. However, CIM pretreatment repressed the level of p-IkBa at 5 and 10 min and delayed the phosphorylation peak from 5 min to 30 min, suggesting that the activation of NF-κB was significantly inhibited by CIM. Moreover, the luciferase reporter assay further demonstrated the impaired NF-κB activation by CIM (Fig. 4C).

In terms of MAPKs signaling, the serial band spectrums of JNK, ERK, p38 and their phosphorylation form were similar between control and CIM-pretreated group, indicating an intact RANKL-induced MAPKs signaling activation after CIM administration.

Collectively, these results proved that CIM inhibited osteoclastogenesis via attenuating the NF-κB signaling without significant effect on MAPKs (JNK, ERK, and p38) signaling pathways.

3.5 CIM Treatment Attenuated Ti Particle-Induced Osteolysis *in Vivo*

Based on the above-mentioned results, we verified the therapeutic effect of CIM for ALP in established Ti particle-induced murine calvarial osteolysis model. As demonstrated by the micro-CT scanning in Fig. 5,extensive bone erosion was observed in vehicle group in contrast with control, whereas the intragastrical CIM treatment significant attenuated the severity of calvarial osteolysis in multiple bone morphometric indexs, including BMD, BV/TV, number of pores as well as percentage of porosity.

Similarly, images of H&E and TRAP staining of sample slices (Fig. 6) further demonstrated remarkable osteolysis in cross section and promoted accumulation of TRAP + osteoclasts in vehicle group relative to the control. Conforming with the morphometric changes of micro-CT imaging, CIM administration considerably protect the calvaria from bone erosion by reducing the size and number of osteoclasts. Taken together, the data from animal experiment further support that CIM treatment could serve as a therapy for Ti particle-induced osteolysis by curbing osteoclastogenesis and bone resorption.

4 Discussion

Most recently, nearly 2.5 million patients who suffer from joint dysfunction caused by diseases such as hip or knee osteoarthritis receive arthroplasty surgery each year around the world [25]. Artificial joint replacement has gained ground as one of the most effective treatment for articular diseases for which conservative approaches failed. This number will continue to rise in the next 20 to 30 years with younger population who prone to higher load of exercise. Moreover, about 5% of patients undergo revision surgery due to ALP during the first 15 years after primary arthroplasty [1]. Thus, ALP secondary to periprosthetic osteolysis causes increasingly problems in this the worldwide.

ALP is one of the most common long-term complication of arthroplasty. It is widely hold that wear-particle-induced osteolysis is the leading cause of ALP after arthroplasty [26]. Specifically, wear particles were phagocytosed by accumulated macrophages and then triggered the over-expression of inflammatory mediators such as IL-1, IL-6, IL-17, TNF-α, M-CSF, MCP-1 (monocyte chemoattractant factor 1), MIP-1α (macrophage inflammatory protein 1 alpha), etc, which promote the differentiation from macrophages to osteoclasts [27; 28]. RANKL, a specifc receptor activator for NF-κB ligand expressed by osteoblasts and osteocytes, serve as another key molecular in osteoclastogenesis [1]. Both of these two manners could cause periprosthetic osteolysis and subsequent ALP [26; 29].

Given the continuous improvement in the material and manufacturing technology though, the ALP seems to be inevitable. To date, nearly all types of debris worn from different interfaces of prosthesis system, including metal, polymethyl methacrylic (PMMA), polyethylene (PE) and ceramics, were reported as causes of periprosthetic osteolysis at varying severity [28; 30]. Therefore, pharmacotherapies targeting osteoclast have drawn high attention.

In the current study, the CIM demonstrated inhibitory effect on osteoclastogenesis *in vitro*. Noncytotoxic CIM repressed osteoclast differentiation in RAW264.7 and BMMs, and alleviated subsequent bone resorption. The impaired formation F-acting ring also confirmed the findings above. Moreover, we discovered that CIM downregulated expression of specific genes in osteoclast, including those involved in regulation of downstream genes expression (Nfatc1, c-Fos and Traf6) [31], bone resorption function (Cathepsin K and Acp5) [32], calcium homeostasis (Calcr) [33], and cell fusion of precursors (Dc-stamp) [34]. Then, we further proved that CIM could protect bone from Ti particle-induced osteolysis *in vivo*. This therapeutic effect for potential ALP treatment were supported by results of both micro-CT scanning and

immunohistochemical assay that CIM dose-dependently mitigated the bone erosion and osteoclast accumulation.

After confirming the anti-osteoclastogenetic property of CIM, we elucidated potential molecular mechanism of it. RANKL specifically bind to the RANK on cytomembrane of osteoclast precursor and then trigger the recruitment of TRAFs and TAK1 binding protein 2 in cytoplasm [35]. The RANKL/RANK/TRAFs complex then activates the phosphorylation of TAK1 (TGF-b-activated kinase 1), which in turn initiates both NF-kB and MAPKs signaling by phosphorylating both IKK complex and MKKs [35; 36]. For one, phosphorylated IKK complex causes cleavage of NF-kB from IkB and the following degradation of IkB [37]. For another, phosphorylated MKKs activated the phosphorylation of JNK, ERK and p38 [38]. The activation of all these signaling pathways contributed to the upregulation of osteoclast specific genes expression. In the current study, we found that CIM inhibits osteoclastogenesis by downregulating the phosphorylation of IkBa in NF-kB signaling pathway, as is shown in Fig. 7.

CIM is kind of chromone first discovered in *Cimicifuga Racemosa* but mainly prepared from the root of *Saposhnikovia Divaricata*, both of which are used in traditional Chinese medicine to treat upper respiratory infection and skin inflammatory diseases with a long history. Previous studies prove that CIM has potential to multiple inflammatory diseases. Liu et al. [14] reported that CIM could mitigate imiquimod-induced psoriasis in murine by oxidative stress and inhibiting inflammation and repress NF-κB and MAPKs (JNK, ERK and p38) signaling in HaCaT cells, in which CIM may inhibit the phosphorylation of IkB, JNK, ERK and p38. Han et al. [12] concluded that CIM could alleviate Lipopolysaccharide-induced Inflammatory Responses of RAW264.7 as a rheumatoid arthritis model via inhibiting the phosphorylation of IkB, ERK and p38 (without detecting JNK) in NF-κB and MAPKs signaling pathways.

In the present study, we demonstrated that CIM inhibited RANKL-induced NF-κB signaling via blocking the phosphorylation of IκBα without affecting JNK, ERK and p38 activation of MAPKs signaling during the osteoclastogenesis. In comparison, previous studies on the bioactivity of CIM suggested different conclusions. For one, Liu et al. [14] reported that CIM ameliorates imiquimod-mediated phosphorylation of NF-κB (IκB and p65) and MAPK (JNK, ERK, and p38) signaling in psoriasis models. For another, Han et al. [12] indicated that CIM exerts inhibitory effect on lipopolysaccharide-induced inflammatory response in RAW264.7 cell by downregulating the generation of p-IκBα, p-p65, p-ERK, and p-p38 of NF-κB and MAPK signaling pathways without detecting the level of JNK. The discrepancy between may result from the diverse cell and animal models and limited exploration of molecular mechanism. Imiquimod and lipopolysaccharide were adopted to established experimental models in studies of Liu et al. and Han et al., which shares identical pathway in the downstream of TRAF6 with RANKL-induced signaling but not in the upstream of it. CIM treatment may alter regulation pattern in the upstream of TRAF6 and in NF-κB pathway simultaneously, which causes different conclusion between studies. In addition, time-dependent changes of NF-κB and MAPKs signaling proteins are absent in studies of Liu et al. and Han et al. Moreover, all these three studies including the present one only investigate the level of signaling proteins in limited number, so it seems impossible to come to an agreement for now.

There are several limitations existing in this study. First, we only investigate the expression of IkB, JNK, ERK, p38 and their phosphorylation forms as key factors in NF-κB and MAPKs signaling pathways. To unravel exact target protein in the cascade and acting site of specific protein, more experiment including Western blotting for upstream signaling proteins, “rescue” experiment and molecular docking assay may be required. Second, homeostasis of bone metabolism inevitably involves opposing bone resorption induced by osteoclast and bone formation induced by osteoblast. M-CSF, RANKL and OPG (osteoprotegerin) that serve as critical modulator of osteoclast formation in bone metabolism were all expressed by osteoblast. Thus, the effect of CIM on osteoblast-induced bone formation is supposed to be explored in future studies. Finally, the adopted Ti particle-induced murine calvarial osteolysis model cannot perfectly simulate ALP in patient. From metal and UHMWPE (ultrahigh-molecular-weight polyethylene) to ceramic and PEEK (polyether-ether-ketone), the myriad of particles worn from interfaces of any kind could contributed the periprosthetic osteolysis of varying severity [39]. With structure of thin cortical bone and little stress bearing, murine calvarium only serve as a defective analogue of ALP in hip or knee joint of human [9]. Even though, this model demonstrates similar pathological change compared with polyethylene particle-induced model and widely used in studies of ALP [36; 40]. Therefore, it is reasonable to establish Ti particle-induced murine calvarial osteolysis model for ALP simulation *in vivo*.

Conclusively, for the first time we demonstrated that CIM could alleviate RANKL-induced osteoclastogenesis and Ti particles-induced osteolysis *in vitro* and *in vivo* via inhibiting NF-κB signaling pathway. The current findings suggests that CIM could serve as a potential drug to treat ALP as well as other osteopathies mediated by excessive osteoclasts, therefore broadening the spectrum of bone-protective natural compounds.

Abbreviations

ALP: Aseptic loosening of prosthesis; BMMs: bone marrow-derived macrophages; BV: bone volume; CIM: cimifugin; c-α-MEM: complete α-MEM; MAPKs: mitogen-activated protein kinases; NF-κB: nuclear factor-κB; PBS: phosphate buffer saline; qRT-PCR: polymerase chain reaction; RANKL: receptor activator of nuclear factor κ B ligand; TRAP: tartrate-resistant acid phosphatase; TV: tissue volume; TRAF6: TNF receptor-associated factor 6.

Declarations

Ethics Approval and Consent to Participate

The protocol was performed in accordance with the recommendations of guiding principles of Animal Care Committee of Central South University and approved by the Animal Care Committee of Central South University.

Consent for Publication

Informed consent was obtained from all patients.

Availability of Data and Material

The datasets generated and/or analyzed in this study are available from the corresponding author upon reasonable request.

Competing Interests

The authors declare that the research was conducted in the absence of any commercial or financial relationships that could be construed as a potential conflict of interest.

Funding

This work was supported by the Science & Technology Department of Hunan Province (Grant number 2019JJ50845; 2019JJ50883; 2020JJ5802) and Health Commission of Hunan Province (Grant number 202104070969).

Author's Contributions

The current study was conceived and designed by PD. All procedures were conducted under the guidance of members of the Laboratory of Orthopaedics at the Second Xiangya Hospital (XH and TL). PD and XH performed *in vitro* experiments and participated in animal studies. JD and TL performed *in vivo* experiments and data collection. JD performed statistical analysis. PD and JD drafted the manuscript. All the authors revised the article critically for intellectual content. All the authors have read and approved the final version of manuscript.

Acknowledgments

The authors would like to thank all members of the Laboratory of Orthopathy at the Second Xiangya Hospital for technical assistance.

References

1. Goodman SB, Gallo J. 2019. Periprosthetic Osteolysis: Mechanisms, Prevention and Treatment. J Clin Med 8.
2. Panegrossi G, Ceretti M, Papalia M, et al. 2014. Bone loss management in total knee revision surgery. Int Orthop 38:419-427.

3. Visgauss JD, Perrin DL, Wilson DA, et al. 2020. Midterm Success of a Custom, Non-Fluted, Diaphyseal, Press-Fit Stem Used With a Tumor Megaprosthesis System. J Arthroplasty 35:1333-1338.
4. Zhang L, Haddouti EM, Welle K, et al. 2020. Local Cellular Responses to Metallic and Ceramic Nanoparticles from Orthopedic Joint Arthroplasty Implants. Int J Nanomedicine 15:6705-6720.
5. Prock-Gibbs H, Pumilia CA, Meckmongkol T, et al. 2021. Incidence of Osteolysis and Aseptic Loosening Following Metal-on-Highly Cross-Linked Polyethylene Hip Arthroplasty: A Systematic Review of Studies with Up to 15-Year Follow-up. J Bone Joint Surg Am Publish Ahead of Print.
6. Sun GJ, Yang SF, Ti YF, et al. 2019. Influence of Ceramic Debris on Osteoblast Behaviors: An In Vivo Study. Orthop Surg 11:770-776.
7. Kim JM, Lin C, Stavre Z, et al. 2020. Osteoblast-Osteoclast Communication and Bone Homeostasis. Cells 9.
8. Walsh MC, Lee J, Choi Y. 2015. Tumor necrosis factor receptor- associated factor 6 (TRAF6) regulation of development, function, and homeostasis of the immune system. Immunol Rev 266:72-92.
9. Hu X, Yin Z, Chen X, et al. 2020. Tussilagone Inhibits Osteoclastogenesis and Periprosthetic Osteolysis by Suppressing the NF-κB and P38 MAPK Signaling Pathways. Front Pharmacol 11:385.
10. He K, Zheng B, Kim CH, et al. 2000. Direct analysis and identification of triterpene glycosides by LC/MS in black cohosh, Cimicifuga racemosa, and in several commercially available black cohosh products. Planta Med 66:635-640.
11. Wang X, Jiang X, Yu X, et al. 2017. Cimifugin suppresses allergic inflammation by reducing epithelial derived initiative key factors via regulating tight junctions. J Cell Mol Med 21:2926-2936.
12. Han B, Dai Y, Wu H, et al. 2019. Cimifugin Inhibits Inflammatory Responses of RAW264.7 Cells Induced by Lipopolysaccharide. Med Sci Monit 25:409-417.
13. Jia Z, Tie C, Wang C, et al. 2019. Perturbed Lipidomic Profiles in Rats With Chronic Cerebral Ischemia Are Regulated by Xiao-Xu-Ming Decoction. Front Pharmacol 10:264.
14. Liu A, Zhao W, Zhang B, et al. 2020. Cimifugin ameliorates imiquimod-induced psoriasis by inhibiting oxidative stress and inflammation via NF-κB/MAPK pathway. Biosci Rep 40.
15. Wu LQ, Li Y, Li YY, et al. 2016. Antinociceptive Effects of Prim-O-Glucosylcimifugin in Inflammatory Nociception via Reducing Spinal COX-2. Biomol Ther (Seoul) 24:418-425.
16. Yao L, Wang S, Wei P, et al. 2019. Huangqi-Fangfeng protects against allergic airway remodeling through inhibiting epithelial-mesenchymal transition process in mice via regulating epithelial derived TGF-β1. Phytomedicine 64:153076.
17. Zhang Q, Tang X, Liu Z, et al. 2018. Hesperetin Prevents Bone Resorption by Inhibiting RANKL-Induced Osteoclastogenesis and Jnk Mediated Irf-3/c-Jun Activation. Front Pharmacol 9:1028.
18. Ouyang Z, Zhai Z, Li H, et al. 2014. Hypericin suppresses osteoclast formation and wear particle-induced osteolysis via modulating ERK signalling pathway. Biochem Pharmacol 90:276-287.

19. Yang D, Liu T, Jiang G, et al. 2020. Senkyunolide H attenuates osteoclastogenesis and postmenopausal osteoporosis by regulating the NF-κB, JNK and ERK signaling pathways. Biochem Biophys Res Commun 533:510-518.
20. Zhu W, Yin Z, Zhang Q, et al. 2019. Proanthocyanidins inhibit osteoclast formation and function by inhibiting the NF-κB and JNK signaling pathways during osteoporosis treatment. Biochem Biophys Res Commun 509:294-300.
21. Zhai Z, Qu X, Yan W, et al. 2014. Andrographolide prevents human breast cancer-induced osteoclastic bone loss via attenuated RANKL signaling. Breast Cancer Res Treat 144:33-45.
22. Ikeda F, Nishimura R, Matsubara T, et al. 2004. Critical roles of c-Jun signaling in regulation of NFAT family and RANKL-regulated osteoclast differentiation. J Clin Invest 114:475-484.
23. Wu C, Wang W, Tian B, et al. 2015. Myricetin prevents titanium particle-induced osteolysis in vivo and inhibits RANKL-induced osteoclastogenesis in vitro. Biochem Pharmacol 93:59-71.
24. Holliday LS, Faria LP, Rody WJ, Jr. 2019. Actin and Actin-Associated Proteins in Extracellular Vesicles Shed by Osteoclasts. Int J Mol Sci 21.
25. Nemeth B, Nelissen R, Arya R, et al. 2021. Preventing VTE following total hip and knee arthroplasty: Is prediction the future? J Thromb Haemost 19:41-45.
26. Howie DW, Neale SD, Haynes DR, et al. 2013. Periprosthetic osteolysis after total hip replacement: molecular pathology and clinical management. Inflammopharmacology 21:389-396.
27. Dyskova T, Gallo J, Kriegova E. 2017. The Role of the Chemokine System in Tissue Response to Prosthetic By-products Leading to Periprosthetic Osteolysis and Aseptic Loosening. Front Immunol 8:1026.
28. Gibon E, Córdova LA, Lu L, et al. 2017. The biological response to orthopedic implants for joint replacement. II: Polyethylene, ceramics, PMMA, and the foreign body reaction. J Biomed Mater Res B Appl Biomater 105:1685-1691.
29. Lin TH, Tamaki Y, Pajarinen J, et al. 2014. Chronic inflammation in biomaterial-induced periprosthetic osteolysis: NF-kappaB as a therapeutic target. Acta Biomater 10:1-10.
30. Merkel KD, Erdmann JM, McHugh KP, et al. 1999. Tumor necrosis factor-alpha mediates orthopedic implant osteolysis. Am J Pathol 154:203-210.
31. Park JH, Lee NK, Lee SY. 2017. Current Understanding of RANK Signaling in Osteoclast Differentiation and Maturation. Mol Cells 40:706-713.
32. Walia B, Lingenheld E, Duong L, et al. 2018. A novel role for cathepsin K in periosteal osteoclast precursors during fracture repair. Ann N Y Acad Sci 1415:57-68.
33. Granholm S, Henning P, Lerner UH. 2011. Comparisons between the effects of calcitonin receptor-stimulating peptide and intermedin and other peptides in the calcitonin family on bone resorption and osteoclastogenesis. J Cell Biochem 112:3300-3312.
34. Kodama J, Kaito T. 2020. Osteoclast Multinucleation: Review of Current Literature. Int J Mol Sci 21.

35. Asagiri M, Takayanagi H. 2007. The molecular understanding of osteoclast differentiation. Bone 40:251-264.
36. Sun Z, Zeng J, Wang W, et al. 2020. Magnoflorine Suppresses MAPK and NF-κB Signaling to Prevent Inflammatory Osteolysis Induced by Titanium Particles In Vivo and Osteoclastogenesis via RANKL In Vitro. Front Pharmacol 11:389.
37. Wada T, Nakashima T, Hiroshi N, et al. 2006. RANKL-RANK signaling in osteoclastogenesis and bone disease. Trends Mol Med 12:17-25.
38. Feng X. 2005. RANKing intracellular signaling in osteoclasts. IUBMB Life 57:389-395.
39. Wooley PH. 2014. How has the introduction of new bearing surfaces altered the biological reactions to byproducts of wear and modularity? Clin Orthop Relat Res 472:3699-3708.
40. Taki N, Tatro JM, Nalepka JL, et al. 2005. Polyethylene and titanium particles induce osteolysis by similar, lymphocyte-independent, mechanisms. J Orthop Res 23:376-383.

Figures

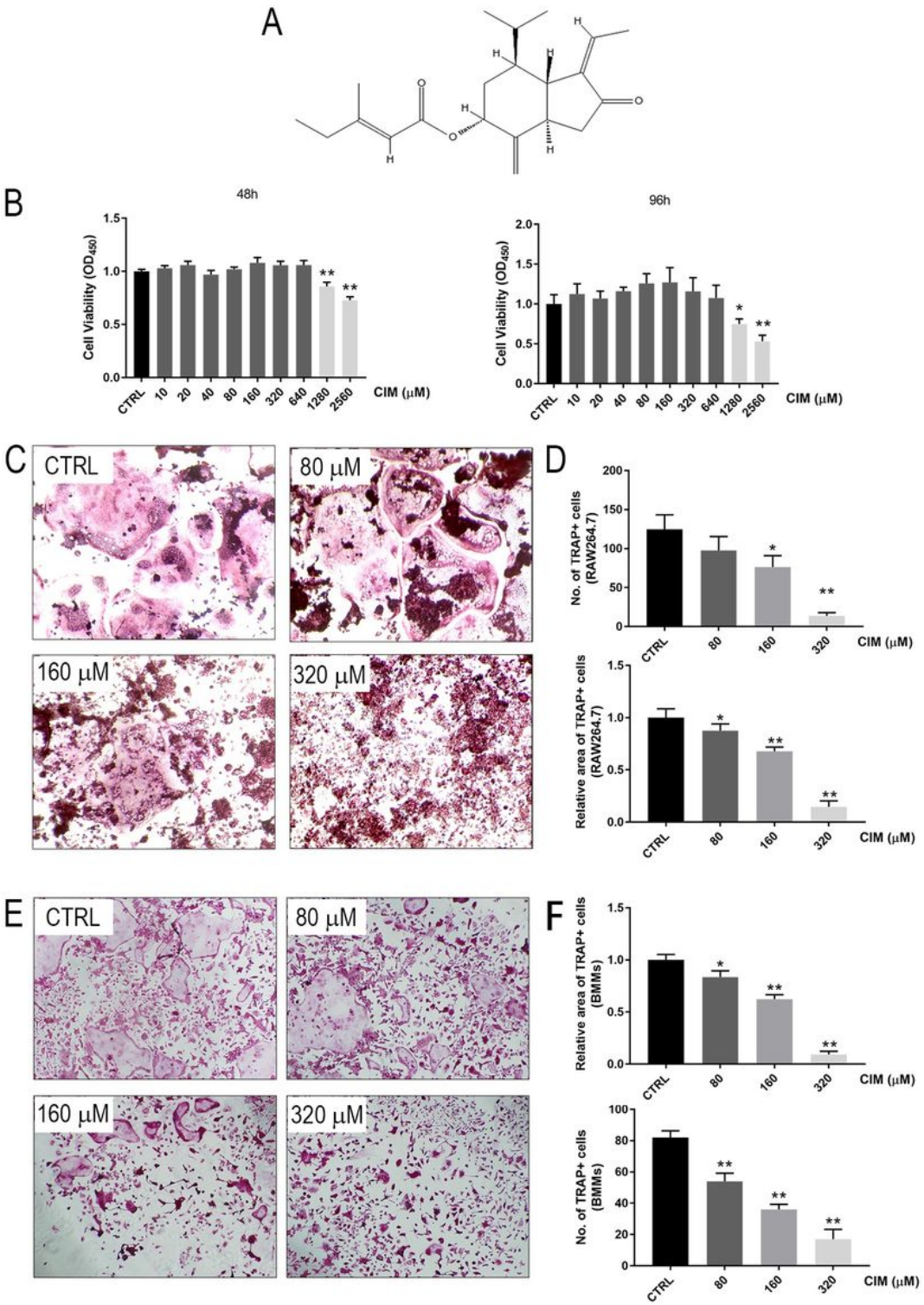

Figure 1

CIM inhibits RANKL-induced osteoclast formation at noncytotoxic dose in a dose-dependent manner in RAW264.7 and BMMs cell lineages. (A) The chemical structure of CIM. (B) The cell viability of BMMs treated with CIM at different doses for 48 or 96 h. CIM less than or equal to 320 μM was identified as noncytotoxic. (C) & (E) The TRAP staining images of RAW264.7 and BMMs cells incubated with CIM of

gradient concentrations for 5-7 days are presented. The numbers (D) and areas (F) of TRAP+ osteoclast were quantified and analyzed. (*: P < 0.05; **: P < 0.01 compared with control group)

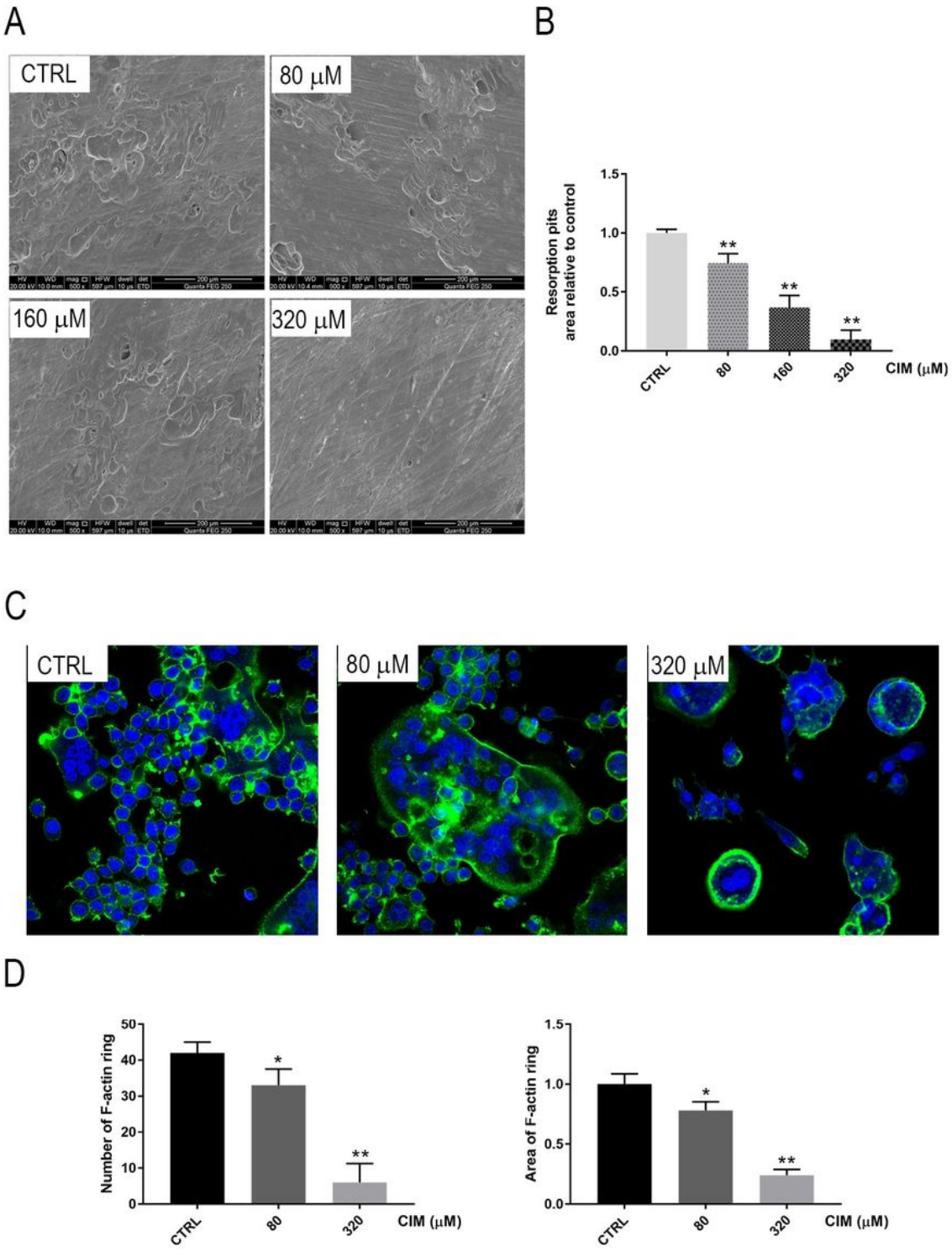

Figure 2

Noncytotoxic CIM dose-dependently mitigates the bone-resorbing activity of osteoclast in vitro. (A) Scanning electron microscope images of eroded surface in bone slices treated with CIM at indicated concentration. (B) Area of bone resorption pits relative to control group were demonstrated. (C)

Immunofluorescence images of F-actin rings (in green) in BMMs-derived osteoclasts treated with CIM at indicated doses. (*: P < 0.05; **: P < 0.01 compared with control group)

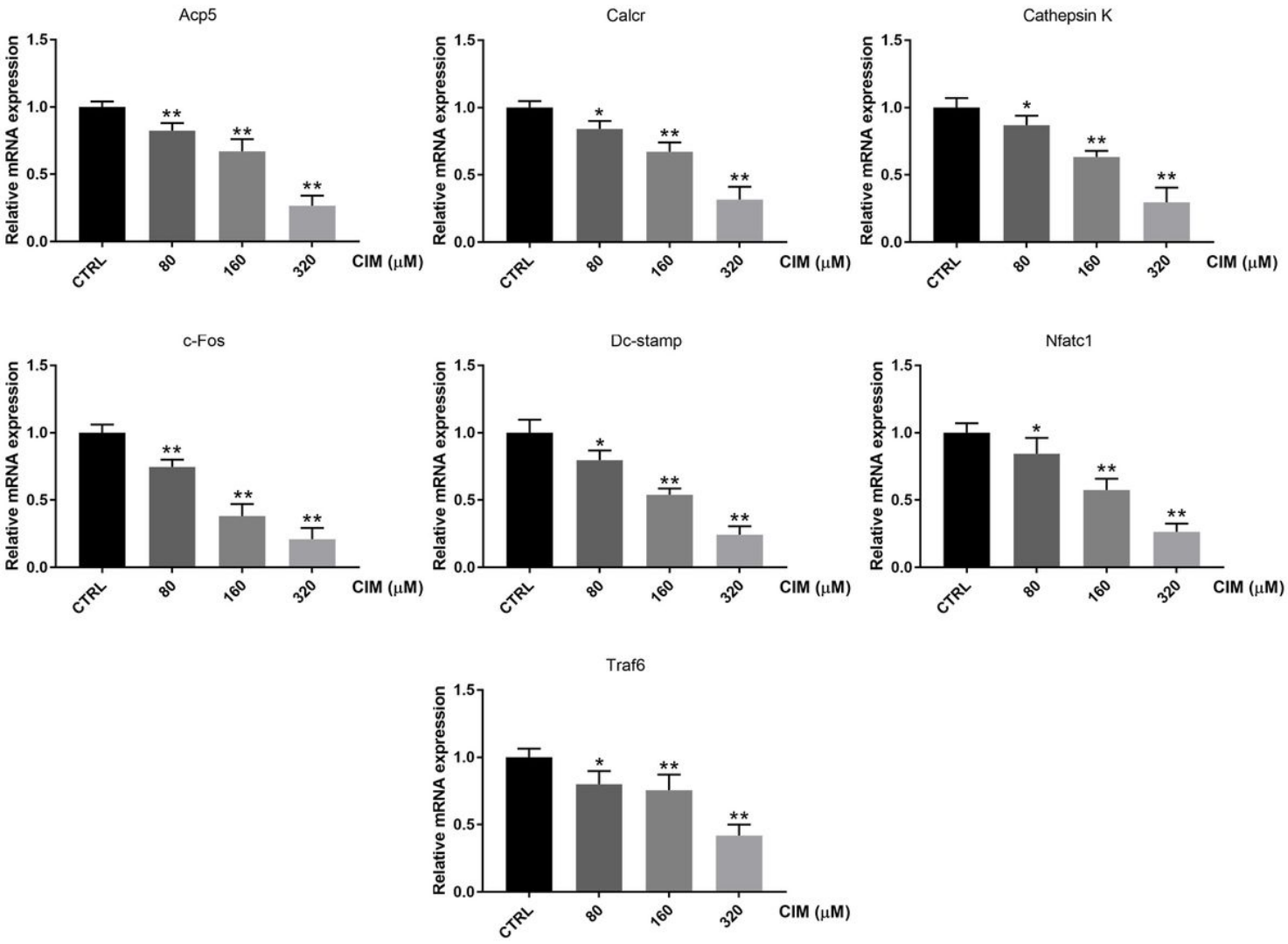

Figure 3

CIM dose-dependently represses the expression level of osteoclast marker genes in RANKL-stimulated osteoclasts, including c-Fos, Nfatc1, Acp5, Calcr, Cathespin K, Dc-stamp and Traf6. These genes were quantified using qRT-PCR and normalized with the level of housekeeping Gapdh. (*: P < 0.05; **: P < 0.01 compared with control group)

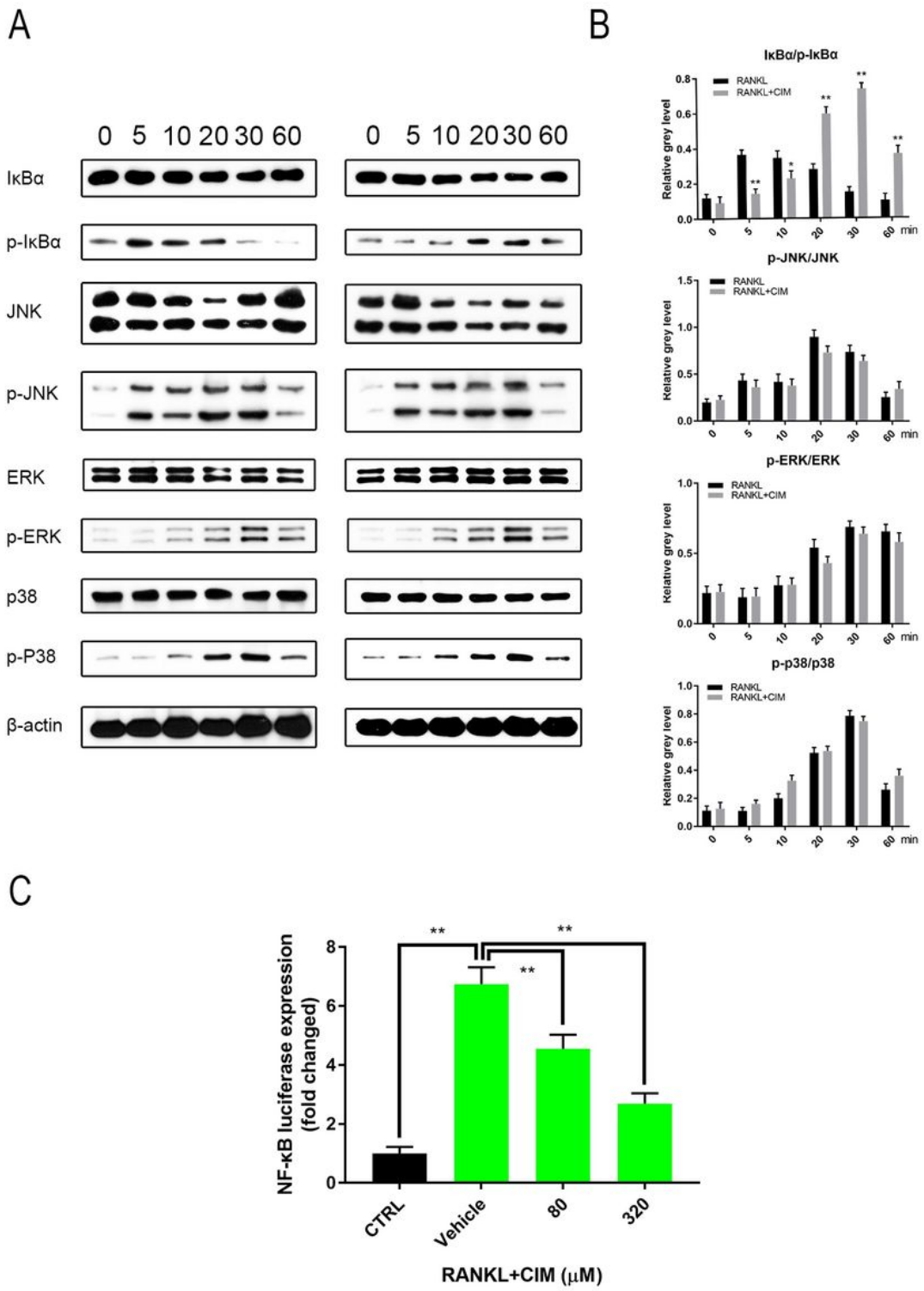

Figure 4

CIM downregulates NF-κB signaling pathway but MAPKs signalings in RANKL-pretreated osteoclast precursors. (A) Chronological Western blotting band spectrum of key factors and their phosphorylation form in NF-κB and MAPKs (JNK, ERK and p38) signaling pathway of BMMs pretreated with 320 μM CIM and RANKL were presented, which was contrasted by control group (only RANKL). (B) The level of phosphorylated NF-κB and MAPKs proteins were normalized using the total level of these proteins and

analyzed. (C) Luciferase activity of RAW264.7 transfected with NF-κB luciferase reporter gene was quantified. (*: P < 0.05; **: P < 0.01 compared with control group)

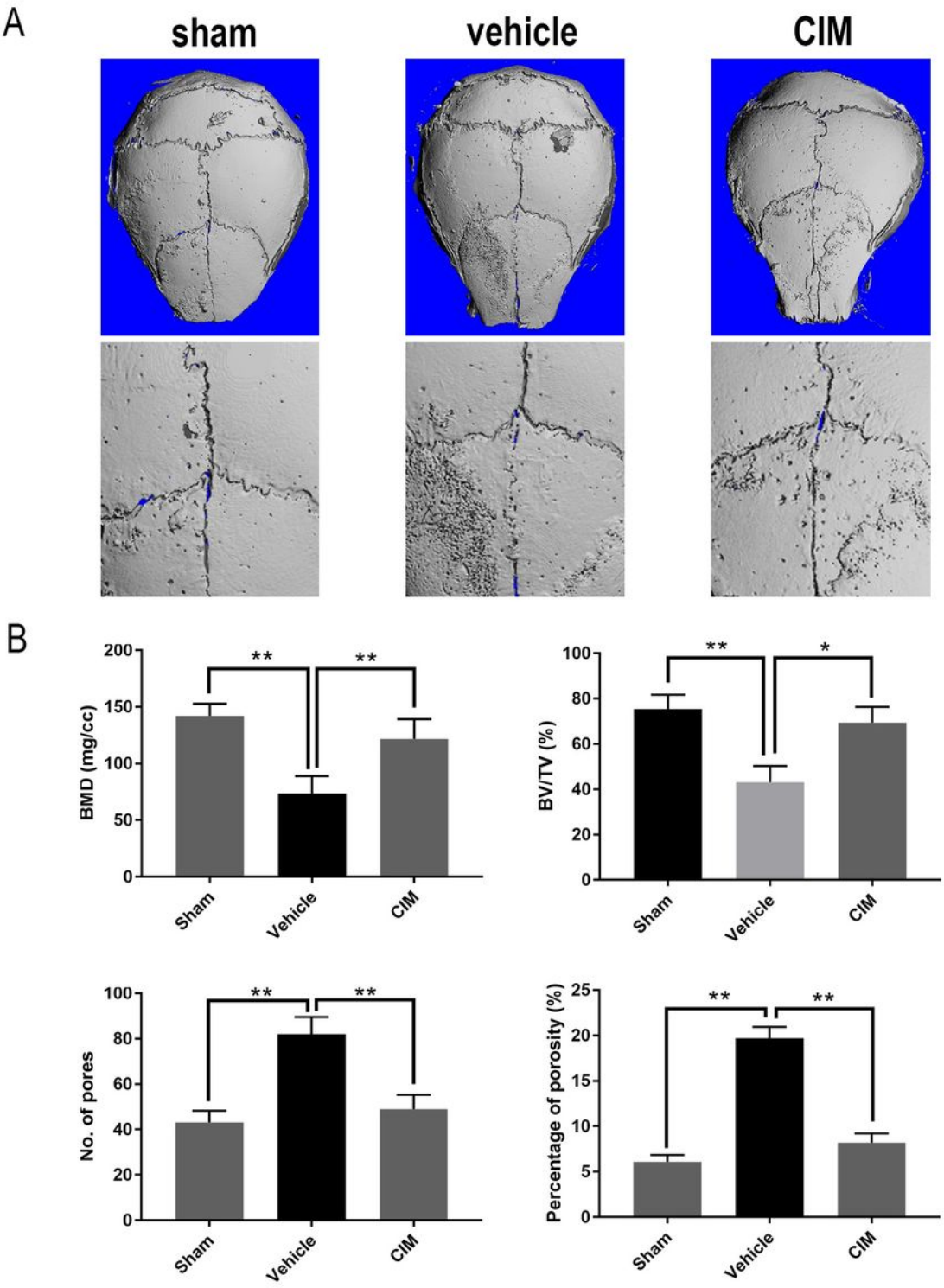

Figure 5

CIM protects murine calvaria from Ti particles-induced osteolysis in vivo. (A) Reconstructed micro-CT radiograph of harvested murine calvaria. (B) Bone mineral density (BMD), bone volume against tissue

volume (BV/TV), the number of pores and percentage of total porosity within regions of interest were analyzed. (*: P < 0.05; **: P < 0.01 versus control group)

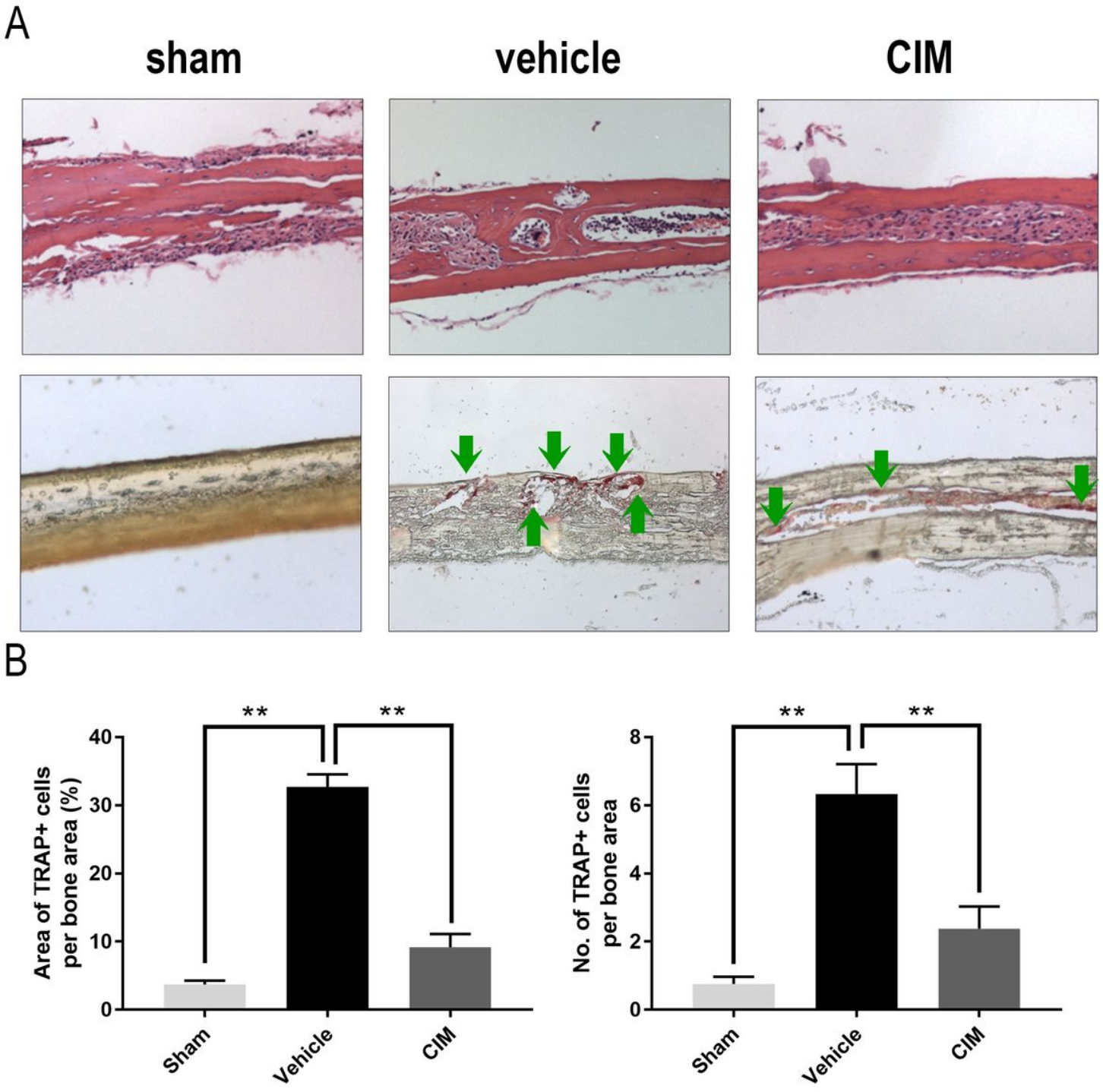

Figure 6

The histological staining shows inhibited bone erosion and osteoclast accumulation in the harvested murine calvaria. (A) Representative images of H&E and TRAP staining (×100) of indicated groups. (B) The diagram and statistical analysis of the area and number of TRAP+ cells per bone region. (**: P < 0.01 versus control group)

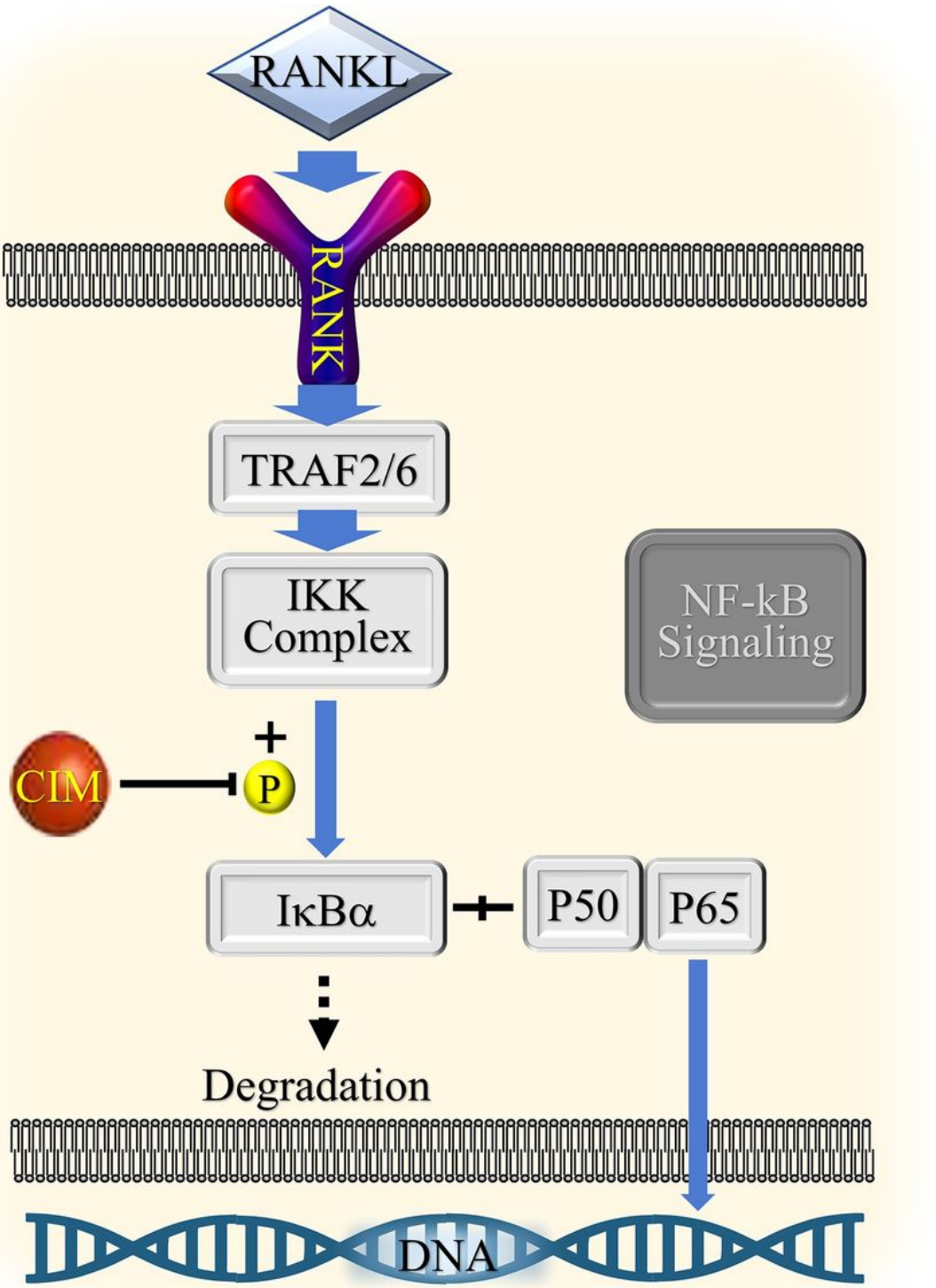

Figure 7

A schematic diagram showing the assumed mechanism of CIM-induced inhibition of NF-κB signaling.